Design of Fuel-Optimal Low-Thrust Trajectories to Service the James Webb Space Telescope

Max Yasgur*
Cornell University, Ithaca, NY, 14853

The James Webb Space Telescope (JWST) is NASA's newest flagship infrared telescope, designed with the goal to peer deeper into the Universe than any instrument before to better understand cosmic development. The telescope follows a near-periodic, nonkeplerian halo orbit about one of the five equilibria in the Sun-Earth dynamical system, L_2, which is about 1.5 million km from Earth and inherently unstable. To maintain this orbit, JWST requires station-keeping burns which limit the life of the mission due to finite propellant reserves. The goal of this work is to replicate the results of a paper out of the Jet Propulsion Lab (JPL) that demonstrated the efficacy of a low-thrust transfer to service JWST while minimizing spent fuel mass. We explore the underlying structure of the dynamics models and formulate the optimal control structure applying Pontryagin's Maximum Principle (PMP). Unfortunately, the results of this work show poor convergence on an optimal trajectory. The discussion section dives into possible sources of optimization infeasibility and next steps are discussed.

I. Introduction

The Hubble Space Telescope (HST) was one of the most transformative space instruments, allowing humanity to observe the visible cosmological structure of the universe billions of lightyears away. Originally launched in 1990, Hubble has been successfully collecting visible light images since 1994, after a primary optical correction by the crew of Space Shuttle mission STS-61. Five HST servicing missions were conducted from 1993-2009. This was made possible due the nominal orbital altitude of the telescope at 540 km above the Earth, putting HST within the low-earth orbit (LEO) regime.

To unlock more insight into the formation of the universe, the James Webb Space Telescope (JWST) sees in infrared (IR) telescope, a region of the electromagnetic spectrum that the human eye cannot detect. Due to the IR optical sensitivity required by JWST to view farther than any telescope prior, the option to orbit near the Earth is unfeasible, as the Earth's albedo would over saturate the instrument's infrared sensors. NASA engineers decided on the second Sun-Earth Lagrange point, L_2, due to its thermal stability. The one potential downside is that L_2 is approximately 3 times further from Earth than the Moon, meaning that the telescope had to be designed without the fallback of a servicing mission in mind. A notable detail about L_2 is that it is unstable, meaning that JWST requires small station-keeping burns roughly every three weeks to maintain its halo orbit. This imposes a mission life constraint, as there is a limit to the onboard propellant which used for the station-keeping maneuvers. This is the inspiration for the project.

Woollands and Eggl [1] demonstrated the efficacy of a low-thrust servicing mission to refuel JWST. My project aims to replicate their results from 2020, namely the construction of an optimal trajectory starting from Earth orbit which rendezvouses with the JWST halo orbit simultaneously minimizing the spent fuel mass by the time it reaches its target.

II. Theoretical Background & Problem Formulation

A. Circular-Restricted Three-Body Problem

The CR3BP assumes a restricted three-body system (s.t. $m_1 > m_2 >> m_P$) where m_1 and m_2 orbit their common barycenter along mutually circular orbits and are unaffected by the gravitational influence of m_P. We will assume P is a spacecraft for our purposes, but it could equivalently be any infinitesimally small object compared to the two primary masses. A consequence of defining the orbits of the primaries as perfect circles is that they orbit their barycenter at a mutually constant rate, n, the mean motion. It, therefore, is common practice to define a rotating body-frame which co-rotates with the two primaries. The body-frame, $\mathcal{B}$, is defined such that both primaries lie along the radial

*Master of Engineering Student, Sibley School of Mechanical & Aerospace Engineering, mby23@cornell.edu

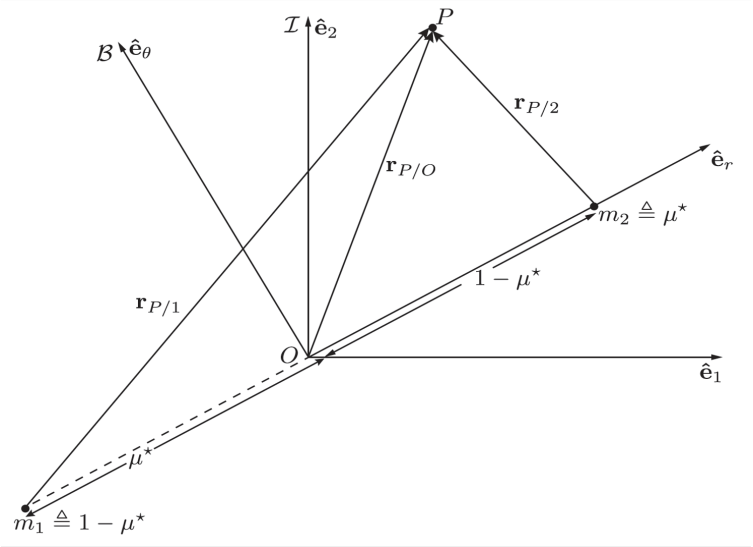

Fig. 1 CR3BP coordinate axes, where O is the barycenter of m_1 and m_2 and $\hat{\mathbf{e}}_3$ (not pictured) is oriented out of the page. Image courtesy of D. Savransky [2].

direction, $\hat{\mathbf{e}}_r$. The rotation axis, $\hat{\mathbf{e}}_3$, is coincident with the inertial frame, $\mathcal{I}$, and $\hat{\mathbf{e}}_\theta$ completes the orthonormal basis set ($\hat{\mathbf{e}}_\theta = \hat{\mathbf{e}}_3 \times \hat{\mathbf{e}}_r$). The coordinates of mass P in the rotating frame are defined as

$$[\mathbf{r}_{P/O}]_{\mathcal{B}} = \begin{bmatrix} x \\ y \\ z \end{bmatrix}.$$

Since $\mathbf{r}_{P/O}$ is the only changing position vector we care about, it is acceptable to drop the subscripts and denote $\mathbf{r} \equiv \mathbf{r}_{P/O}$

NOTE: Canonical Units

Another common practice in within the scope of the CR3BP is define a set of canonical units to simplify much of the later computations. The canonical unit set is defined such that G = 1. Additionally, 1 mass unit (MU) = $m_1 + m_2$, 1 distance unit (DU) = $\|\mathbf{r}_{1/2}\|$, and 2π time units (TU) = $T_{p,1,2}$ (the orbital period of m_1 and m_2) [2]. From these definitions, $n = 1$ per Kepler's Third Law. By nondimensionalizing the problem, we are able to scale the problem to a dependence on a single parameter, the mass parameter,

$$\mu^* = \frac{m_2}{m_1 + m_2}.$$

For the Sun-Earth system, $\mu^* \approx 3.0025 \times 10^{-6}$, 1 DU $\approx$ 1.0004 AU, 1 TU $\approx$ 58.134 days [3].

The equations of motion for this system are given by [3]

$$\ddot{x} = -\frac{\partial U}{\partial x} + 2\dot{y} \tag{1}$$

$$\ddot{y} = -\frac{\partial U}{\partial y} - 2\dot{x} \tag{2}$$

$$\ddot{z} = -\frac{\partial U}{\partial z}. \tag{3}$$

where $U \triangleq -\left(\frac{1-\mu^*}{r_1} + \frac{\mu^*}{r_2}\right) - \frac{1}{2}(x^2 + y^2)$ is a scalar pseudo-potential associated with both the aggregate gravitational field induced by the two primaries and the fictitious centrifugal potential which arises from the rotating reference frame convention. Additionally, $r_1 \triangleq \|\mathbf{r}_{P/1}\| = \sqrt{(x+\mu^*)^2 + y^2 + z^2}$ and $r_2 \triangleq \|\mathbf{r}_{P/2}\| = \sqrt{(x-(1-\mu^*))^2 + y^2 + z^2}$ are the

distances between the spacecraft and the respective primary. Koon et al. (2011) details three derivations of the above equations (Eqn.1-3) in the Newton, Lagrangian, and Hamiltonian frameworks [3].

As it will prove useful in solving the ODEs, it is also customary to reformulate Eqns.(1-3) in state-space form, where we define the state $\mathbf{x} = [x \;\; y \;\; z \;\; v_x \;\; v_y \;\; v_z]^T$. The second-order ODEs can then be rewritten in the form

$$\dot{\mathbf{x}} = \begin{bmatrix} \dot{\mathbf{r}} \\ \dot{\mathbf{v}} \end{bmatrix} = \begin{bmatrix} \mathbf{v} \\ \mathbf{g}(\mathbf{r}) + \mathbf{h}(\mathbf{v}) \end{bmatrix}, \tag{4}$$

where the functions $\mathbf{g}(\mathbf{r})$ and $\mathbf{h}(\mathbf{v})$ are defined in [3] as

$$\mathbf{g}(\mathbf{r}) = \begin{bmatrix} x - (1-\mu)(x+\mu)/r_1^3 - \mu(x+\mu-1)/r_2^3 \\ y - (1-\mu)y/r_1^3 - \mu y/r_2^3 \\ -(1-\mu)z/r_1^3 - \mu z/r_2^3 \end{bmatrix}, \tag{5}$$

$$\mathbf{h}(\mathbf{v}) = \begin{bmatrix} 2v_y \\ -2v_x \\ 0 \end{bmatrix}. \tag{6}$$

1. Jacobi Constant

Since the equations of motion of the CR3BP are Hamiltonian and independent of time, this equates to the existence of an integral of motion [3]. If we express a quantity akin to the total energy of the system as the sum of the kinetic energy and the pseudo-potential

$$E(x, y, z, \dot{x}, \dot{y}, \dot{z}) = \frac{1}{2}(\dot{x}^2 + \dot{y}^2 + \dot{z}^2) + U(x, y, z), \tag{7}$$

it is trivial to show that differentiating with respect to time results in zero on the right hand side. The argument of the derivative is therefore is a constant, and we can define what is known as the Jacobi constant as

$$C \triangleq \frac{1}{2}(\dot{x}^2 + \dot{y}^2 + \dot{z}^2) + U(x, y, z). \tag{8}$$

The Jacobi constant is the only conserved quantity of the CR3BP, though it is not an energy integral because neither energy nor angular momentum are independently conserved. Instead, the two are in a constant trade-off for all time. Despite the Jacobi constant being the only conserved quantity or integral of the CR3BP, meaning we cannot solve for the exact state of the spacecraft, we are still able to define regions where the spacecraft is able to traverse and regions where the spacecraft cannot. The boundaries of these *forbidden* regions can be plotted against their Jacobi constant value to form a surface known as a zero-velocity surface, as shown in Fig. 2.

B. Manifold Dynamics

Thorough discussions of invariant manifolds and stable structures are provided in Koon et al. (2011), Koleman et al. (2012), and Gómez et al. (2001) [3–5]. In an attempt to distill the fundamentals, we focus on the Sun-Earth L_2. The phase space of the spatial CR3BP is six-dimensional (3 position, 3 velocity states). If we examine near L_2 in phase space, Gómez et al. (2001) showed that this equilibrium is of type center × center × saddle by evaluating the eigenvalues of the Jacobian of the pseudopotential near this point. If we move off of the Lagrange point by a small distance, we are able to linearize the dynamics of a particle in its vicinity. This gives rise to vertical and planar Lyapunov orbits, which are one-parameter families of periodic orbits, characterized by their energy, h. By increasing h and traversing further from the Lagrange point, so that the linearization is less robust, it is possible to extend the Lyapunov family to other classes of periodic orbits.

First discovered in the late 60s by Farquhar, a halo orbit belongs to a family of periodic orbits which have the key feature of being symmetrical about the y=0 plane [5]. A third-order expansion of the nonlinear equations governing the periodic motion of a halo orbit was derived by Richardson [6]. Using this third-order model to generate initial conditions, a specified halo orbit can be constructed using the method of differential correction, as laid out by Howell in her dissertation [7]. Although they are periodic, halo orbits are inherently unstable due the associated eigenvalues

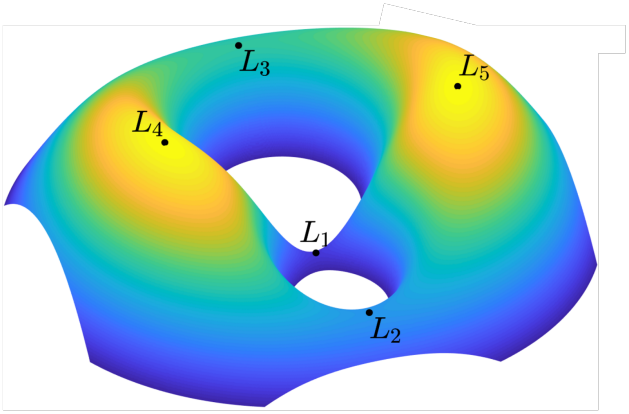

Fig. 2 A plot of the zero-velocity surface associated with the Jacobi constant for $\mu^* = 0.3$. An increased Jacobi constant corresponds to a lower the height on the surface. The locations of the five Lagrange points are also visualized. Image courtesy of D. Savransky [2].

of the of the L_2 equilibrium, and in particular the saddle component. A small deviation from the halo leads to a hyperbolically asymptotic divergence away from the structure, following what is known as the unstable manifold [1]. Somewhat counterintuitively, since the structure is time invariant, a push onto the inverse structure, the stable manifold, will converge onto the halo. These stable and unstable manifolds generate tube-like structures which converge to and diverge from a set of points on a given halo, respectively. Fig. 3 shows these tube-like structures and the associated flow directions.

C. Controlled Restricted Three-Body Problem

We can extend the circular restricted three body problem to also include a propulsion model. In this case, we need to augment our state vector to include the spacecraft mass, m, such that $\mathbf{x} = [x \;\; y \;\; z \;\; v_x \;\; v_y \;\; v_z \;\; m]^T$. Per the form provided in [8], the equations of motion can be expressed by

$$\dot{\mathbf{x}} = \begin{bmatrix} \dot{\mathbf{r}} \\ \dot{\mathbf{v}} \\ \dot{m} \end{bmatrix} = \begin{bmatrix} \mathbf{v} \\ \mathbf{g}(\mathbf{r}) + \mathbf{h}(\mathbf{v}) + uT_{max}\boldsymbol{\alpha}/m \\ -uT_{max}/c \end{bmatrix}, \tag{9}$$

where T_{max} is the maximum thrust magnitude of the propulsion model, c is the exhaust velocity of the engine, u is the throttle level ($0 \leq u \leq 1$), and $\boldsymbol{\alpha}$ is the unit vector describing the thrust direction. In this problem, u and $\boldsymbol{\alpha}$ are the control variables. We will show in the next section how we can reduce the control variables to only u by employing Pontryagin's Maximum Principle (PMP). Our goal now is to devise an optimization strategy to minimize the fuel usage along the trajectory.

D. Construction of the Shooting Function

Generally, a trajectory optimization problem is posed as the following: we have some state vector $\mathbf{x}$, control inputs $\mathbf{u}$, and constant parameters $\mathbf{p}$. The dynamics of the system can be written as some vector-valued function $\dot{\mathbf{x}} = \mathbf{f}(\mathbf{x}(t), \mathbf{u}(t), \mathbf{p}, t)$, and we have specified conditions at the start and end of the trajectory, ψ_0, ψ_f. There also exist constraints on the system, both in the control and the state. We are then trying to minimize some cost function J such that we satisfy our constraints along the whole trajectory. The problem at hand is known as optimal control, and we are trying to find some control u which minimizes J. Most generally, the problem statement is expressed:

$$\arg\min_{\mathbf{u}} \; J = \phi(\mathbf{x}(t_f), t_f) + \int_{t_0}^{t_f} \mathcal{L}(\mathbf{x}, \mathbf{u}, t)dt, \tag{10}$$

where $\phi(\mathbf{x}(t_f), t_f)$ is a terminal cost, and $\mathcal{L}(\mathbf{x}, \mathbf{u}, t)$ is the Lagrangian of the system. In the case of fuel-minimization, the cost function takes on the form:

$$J = \frac{T_{max}}{c} \int_{t_0}^{t_f} u dt, \tag{11}$$

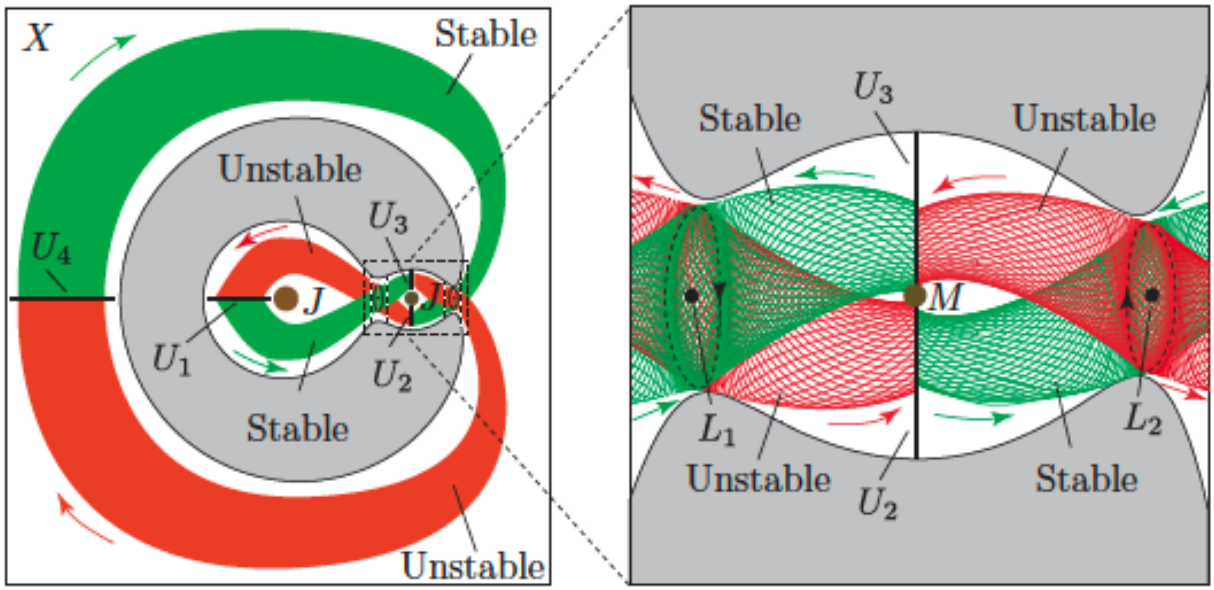

Fig. 3 Stable and unstable manifolds are shown in green and red, respectively. The arrows denote the flow of a particle on a given structure. Figure taken from Koon et al. (2011) [3]

where t_0 and t_f are the initial and final times, respectively. Here, the throttle u is a typical stand-in for the mass-flow rate of the propulsion system which is equal to the Lagrangian. There are no specified terminal costs for this problem. In the fuel-optimal case, the control structure takes on bang-bang control such that the throttle is binary, either on (1) or off (0). This leads to discontinuities that cause a lot of problems for numerical integrators around the switching points [9]. We introduce two different smoothing techniques, the first of which augments the cost function using a homotopic method between fuel optimal and energy optimal [10]. The cost function changes to

$$J = \frac{T_{max}}{c} \int_{t_0}^{t_f} [u - \varepsilon u(1-u)]dt, \quad \varepsilon \in [0,1]. \tag{12}$$

Due to the reduction in harsh discontinuities, the energy-optimal problem ($\varepsilon = 1$) is solved first and used as a seed for future trajectories. Once the energy-optimal solution is acquired, ε is gradually decreased for successive transfers until it obtains a value of zero, in which case the following trajectories use bang-bang control. Jiang et al. (2012) [10] has an illustrative figure showing the effect of variable ε on the throttle over their whole trajectory which can be seen in Fig. 4.

From the cost function in Eq.12 alone, the optimization is ill-constrained for the problem, since it lacks any information about the rest of the state. Importantly, the dynamics are also a constraint that must be satisfied at times in the optimization [11].

In order to incorporate the cost function into the numerical integration of the equations of motion, we need to form the Hamiltonian for this system. The Hamiltonian is defined by $\mathcal{H} \equiv \mathcal{L}(\mathbf{x}, \mathbf{u}, t) + \boldsymbol{\lambda}^T \mathbf{f}$, where λ is a vector of Lagrange multipliers, commonly referred to as costates. The costates form the solutions to the adjoint equations of the system. For this problem, the Hamiltonian can be expressed as

$$\mathcal{H} = \boldsymbol{\lambda}_r \cdot \mathbf{v} + \boldsymbol{\lambda}_v \cdot [\mathbf{g}(\mathbf{r}) + \mathbf{h}(\mathbf{v}) + \frac{uT_{max}}{m}\boldsymbol{\alpha}] - \lambda_m \frac{uT_{max}}{c} + \frac{uT_{max}}{c}[u - \varepsilon u(1-u)], \tag{13}$$

Each state has a corresponding costate, thus $\boldsymbol{\lambda} = [\lambda_x \ \ \lambda_y \ \ \lambda_z \ \ \lambda_{v_x} \ \ \lambda_{v_y} \ \ \lambda_{v_z} \ \ \lambda_m]$. The costate dynamics arise from applying the Euler-Lagrange equations to J. We obtain two sets of differential equations that impose further conditions on the system to reach optimality. Adopting the notation of [10], the conditions read

$$\dot{\boldsymbol{\lambda}} = \left(\frac{\partial \mathcal{H}}{\partial \mathbf{x}}\right)^T = \begin{bmatrix} \dot{\boldsymbol{\lambda}}_r \\ \dot{\boldsymbol{\lambda}}_v \\ \dot{\lambda}_m \end{bmatrix} = \begin{bmatrix} -\mathbf{G}^T \boldsymbol{\lambda}_v \\ -\boldsymbol{\lambda}_r - \mathbf{H}^T \boldsymbol{\lambda}_v \\ uT_{max}/m^2 \boldsymbol{\lambda}_v \cdot \boldsymbol{\alpha} \end{bmatrix}, \tag{14}$$

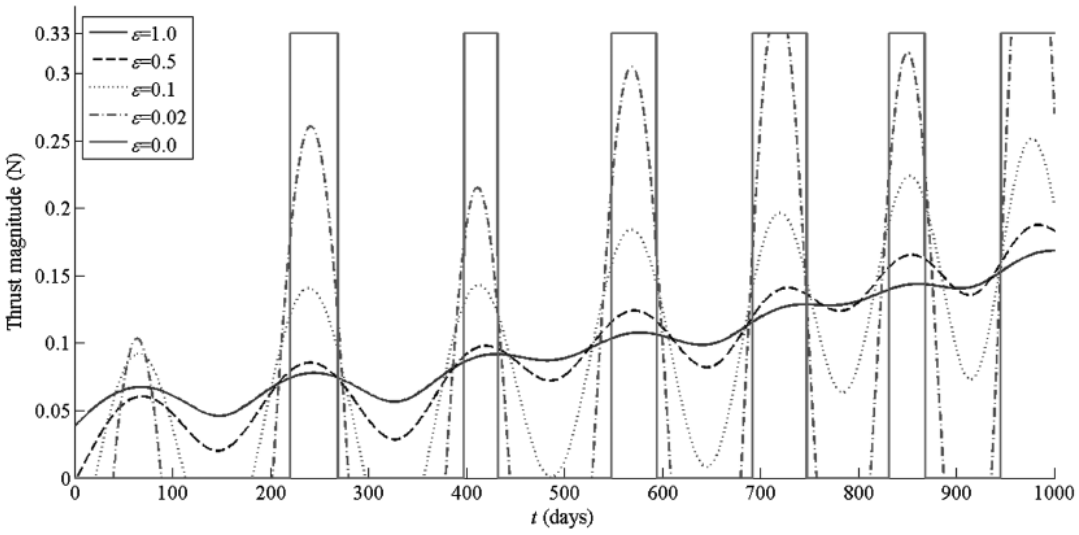

Fig. 4 Optimal thrust profile for decreased ε. Figure taken from Jiang, et al. (2012) [10]

where $\mathbf{G} = \partial \mathbf{g}(\mathbf{r})/\partial \mathbf{r}$ and $\mathbf{H} = \partial \mathbf{h}(\mathbf{v})/\partial \mathbf{v}$, and

$$\left(\frac{\partial \mathcal{H}}{\partial \mathbf{u}}\right)^T = 0. \tag{15}$$

According to Woollands et al. (2020), we can employ Pontryagin's Maximum Principle to $\mathcal{H}$ to find a form for the optimal control inputs denoted by a superscript '*'. The optimal thrust vector is found via

$$\boldsymbol{\alpha}^* = \arg\min_{\|\boldsymbol{\alpha}\|} \mathcal{H}. \tag{16}$$

They continue to show that by minimizing the Hamiltonian, the optimal thrust vector takes the form

$$\boldsymbol{\alpha}^* = -\frac{\boldsymbol{\lambda}_v}{\|\boldsymbol{\lambda}_v\|}. \tag{17}$$

Repeating the a similar process to find the optimal throttle has us minimize the argument to the following:

$$-\frac{T_max}{c}\left[\frac{c\|\boldsymbol{\lambda}_v\|}{m} + \lambda_m - 1\right] u. \tag{18}$$

We then define the term inside the brackets as a switching function, S. The optimal throttle u^* can therefore be expressed as a function of S:

$$u^*(S) = \begin{cases} 0 & \text{if } S > \varepsilon \\ \frac{1}{2}\left[1 - \tanh\frac{S}{\rho}\right] & \text{if } -\varepsilon \leq S \leq \varepsilon \\ 1 & \text{if } S < \varepsilon \end{cases}, \tag{19}$$

where ρ is a second smoothing parameter used to parameterize the continuously differentiable structure in the inner interval. Adopting a second smoothing method has the upside that switching detection can be avoided but the downside that true bang-bang control will never be reached. Following Woollands, they sweep ρ from 1 to 10^-5 with the intention of developing sharper switching as ρ tends to zero while still maintaining continuity.

Now that we have forms for our optimal control inputs, we define a new state vector $\mathbf{y}$ as a concatenated vector of

our states and costates, $\mathbf{y} = [\mathbf{x}^T \;\; \boldsymbol{\lambda}^T]^T$. The complete dynamics model is now

$$\dot{\mathbf{y}} = \mathbf{F}(\mathbf{y}) = \begin{bmatrix} \dot{\mathbf{r}} \\ \dot{\mathbf{v}} \\ \dot{m} \\ \dot{\boldsymbol{\lambda}}_r \\ \dot{\boldsymbol{\lambda}}_v \\ \dot{\lambda}_m \end{bmatrix} = \begin{bmatrix} \mathbf{v} \\ \mathbf{g}(\mathbf{r}) + \mathbf{h}(\mathbf{v}) + (\boldsymbol{\lambda}_v/\lambda_v)uT_{max}/m \\ -uT_{max}/c \\ -\mathbf{G}^T\boldsymbol{\lambda}_v \\ -\boldsymbol{\lambda}_r - \mathbf{H}^T\boldsymbol{\lambda}_v \\ -\lambda_v uT_{max}/m^2 \end{bmatrix}. \tag{20}$$

At its heart, the fuel-optimal transfer problem is a two-point boundary value problem (TPBVP), meaning that we must satisfy the boundary conditions imposed in the problem formulation. For this project, we select an initial position and velocity along a geosynchronous orbit (GEO), a final target position and velocity on the nominal JWST halo orbit, and begin with a fully-filled spacecraft. Due to the nature of the problem, the final mass is a free variable, meaning the associate costate is zero at $t = t_f$. The boundary conditions can be therefore be read

$$\mathbf{r}(t_0) - \mathbf{r}_0 = 0, \qquad \mathbf{v}(t_0) - \mathbf{v}_0 = 0, \qquad m(t_0) - 1 = 0, \tag{21}$$

$$\mathbf{r}(t_f) - \mathbf{r}_f = 0, \qquad \mathbf{v}(t_f) - \mathbf{v}_f = 0, \qquad \lambda(t_f) = 0, \tag{22}$$

where the initial mass has been scaled to one. For the mass to be nondimensionalized in a different unit set than the primaries, we need to nondimensionalize the thrust as well. Defining 1 spacecraft mass unit (MU) as the initial wet mass of the spacecraft, the thrust is now expressed as $T_{max} = 1000MU\ DU/TU^2$, which converts the thrust from newtons into the spacecraft unit system.

Getting back to the optimization framework, we would be able to solve this optimization problem easily if the initial costate vector $\boldsymbol{\lambda}_0$ was given. The optimal throttle could be calculated in the integration and the necessary boundary conditions would be met. Unfortunately, $\boldsymbol{\lambda}_0$ is not provided to us, which means we need to guess. Should the initial guess not satisfy the terminal conditions, we need to change the guess using information about the delta at the end of the trajectory, as well as the Jacobian of the dynamics to get a sense of the local gradients, thus we iterate. This process would be nearly impossible to do manually via guess-and-check. Instead, we define a shooting function $\boldsymbol{\Psi}(\boldsymbol{\lambda})$ as a set of seven equality constraints given in Eqn.22, such that $\boldsymbol{\Psi}(\boldsymbol{\lambda}_0) = 0$ at the end of the trajectory.

III. Simulation Setup

A. Halo Construction

Before we are able to optimize our trajectory, we need to determine our terminal state. This means generating a halo orbit that provides a good estimate of the nominal halo about which JWST orbits. To do this, we employ the differential correction method mentioned prior. In his Master's thesis, Ethan Geipel makes use of his mentor Dr. Kathleen Howell's work to generate a nominal periodic halo from the third order Richardson approximation which is then differentially corrected [7, 12]. Howell takes advantage of the planar symmetry of the periodic halo, and notes that at $y = 0$, the x and z velocity components are zero. The algorithm essentially integrates the three-body equations of motion until the sign of the y component changes, at which point, a differential correction, is applied to a pair of states, either z_0 and $\dot{y}_0$ or x_0 and $\dot{y}_0$. The respective differential corrections can be calculated with the following differential equations:

$$\begin{pmatrix} \delta\dot{x} \\ \delta\dot{z} \end{pmatrix} = \left[\begin{pmatrix} \Phi_{43} & \Phi_{45} \\ \Phi_{63} & \Phi_{65} \end{pmatrix} - \frac{1}{\dot{y}} \begin{pmatrix} \ddot{x} \\ \ddot{z} \end{pmatrix} \begin{pmatrix} \Phi_{23} & \Phi_{25} \end{pmatrix} \right] \begin{pmatrix} \delta z_0 \\ \delta\dot{y}_0 \end{pmatrix} \tag{23}$$

$$\begin{pmatrix} \delta\dot{x} \\ \delta\dot{z} \end{pmatrix} = \left[\begin{pmatrix} \Phi_{41} & \Phi_{45} \\ \Phi_{61} & \Phi_{65} \end{pmatrix} - \frac{1}{\dot{y}} \begin{pmatrix} \ddot{x} \\ \ddot{z} \end{pmatrix} \begin{pmatrix} \Phi_{21} & \Phi_{25} \end{pmatrix} \right] \begin{pmatrix} \delta x_0 \\ \delta\dot{y}_0 \end{pmatrix}, \tag{24}$$

where Φ_{ij} is the $(i, j)^{th}$ entry of the 6×6 state transition matrix formed by

$$\Phi = \begin{bmatrix} 0_{3\times3} & I_3 \\ \mathbf{H}_U & \mathbf{H} \end{bmatrix}, \tag{25}$$

where $\mathbf{H}_U$ is the Hessian of the pseudopotential, and $\mathbf{H}$ is the same defined under Eqn.14. The solutions to the differential correction equations are added to the initial conditions. The procedure iterates until the errors in x and z velocity reach machine precision, although Howell only specifies 10^{-8} at a half period ($y = 0$) [7, 12] .

To match the JWST halo, the true trajectory was pulled from the JPL Horizons site, and manual tweaks were made to the initial Richardson approximation until the differential correction algorithm returned a periodic orbit that was sufficiently close. The comparisons between the true JWST trajectory and the nominal orbit are shown in Fig.5. Additionally, a three axis view of each plane of the generated halo is shown in Fig.6, with styling cues from Koon et al. (2011) [3].

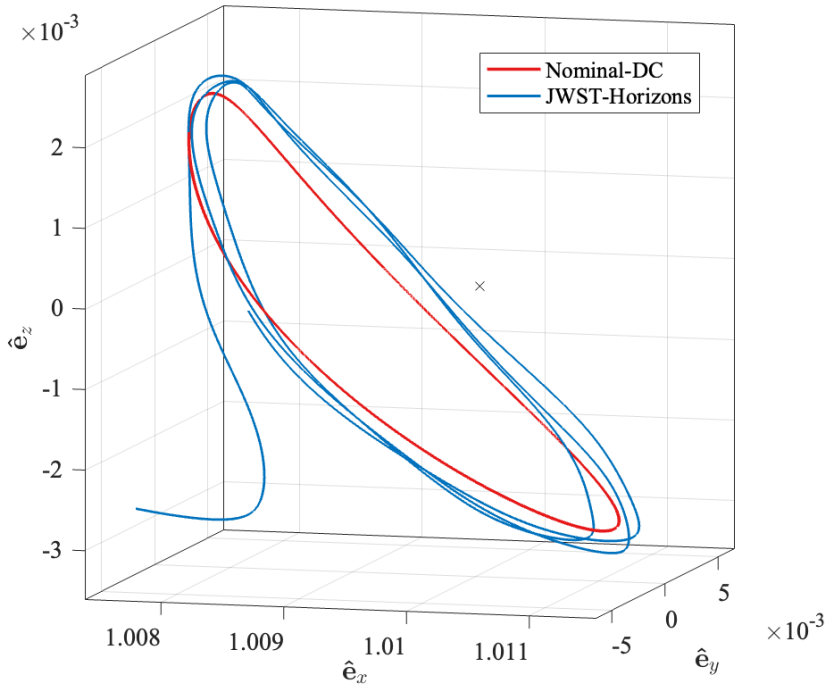

Fig. 5 Nominal, differentially-corrected halo orbit for James Webb Space Telescope (red) overlayed on top of JPL Horizons data of the actual trajectory (blue) in rotating reference frame. Sun-Earth L_2 shown as a small black $\times$. Axes scale is in canonical distance units.

Once the halo was generated, it was relatively simple to construct the associated stable and unstable manifolds. Given the state vector for each point along the halo, a small perturbation of 1×10^{-6} was added to the y-velocity, forming the initial conditions to a forward-time numerical integration of the three-body equations of motion. This produced the local unstable manifold from a given point on the halo. Then, another integration was performed backwards in time with the same initial conditions, thus forming the stable manifold. This was done for each point in the halo. Figs.7a and 7b show the generated stable and unstable manifolds for a nonfull set of halo points.

B. Optimization Method

The trajectory optimization utilized a single shooting approach wherein the initial and final states are the boundary conditions of interest. Following Zhang et al. (2015), we computed the state transition matrix (STM) of the complete dynamics model in Eqn.20, with the intention of improving the robustness of the shooting procedure [8]. The STM, expressed as $\Phi(t_0, t) = d\Psi(\mathbf{y}, t_0, t)/d\mathbf{y}$, is a linearization of the dynamics around time t_0 and acts to map small local variations in the selected initial condition to time t along the trajectory. The STM follows the variational equation

$$\dot{\Phi}(t_0, t) = D_{\mathbf{y}}\mathbf{F}\Phi(t_0, t), \quad \Phi(t_0, t_0) = I_{14\times14}, \tag{26}$$

where $D_{\mathbf{y}}\mathbf{F}$ is the Jacobian of Eqn.20 and was computed using MATLAB's Symbolic Toolbox. Due to $\mathbf{y}$ being 14-dimensional, Eqn.26 is equivalent to 196 first-order ODEs which need to be integrated simultaneously with the

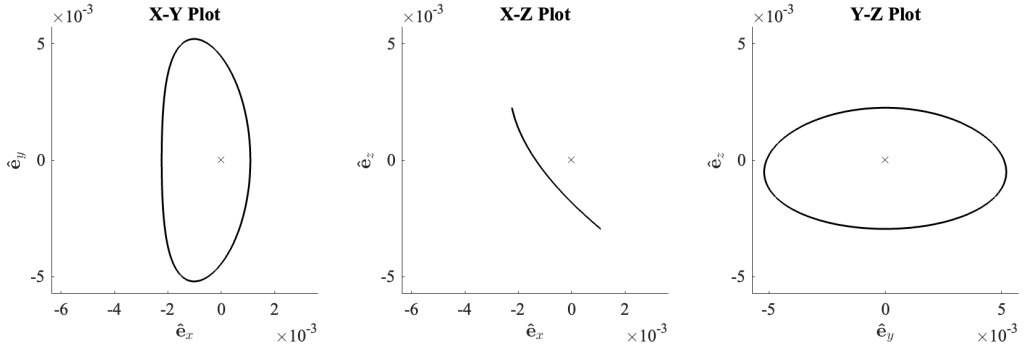

Fig. 6 Three planar views of the nominal differentially-corrected halo orbit of JWST used to define the target (i.e., terminal position and velocity).

Table 1 Units and Constants

Unit	Value
Mass parameter μ	3.0035×10^{-6}
Distance unit (DU)	1.49598×10^{8} km
Time unit (TU)	3.156×10^{7} s
Velocity unit (VU)	29.783 km/s
Mass unit (MU)	400 kg
Maximum thrust magnitude (T_{max})	0.25 N
Exhaust velocity (c)	29.4198 km/s

dynamics. Continuing with Zhang's notation, they define a new state $\mathbf{z}$ as the stack of $\mathbf{y}$ and the columns of Φ, resulting in the equation

$$\dot{\mathbf{z}} = \mathcal{F}(\mathbf{z}) = \begin{bmatrix} \dot{\mathbf{y}} \\ \text{vec}(\dot{\Phi}) \end{bmatrix} = \begin{bmatrix} \mathbf{F}(\mathbf{y}) \\ \text{vec}(D_{\mathbf{y}}\mathbf{F}\Phi) \end{bmatrix}, \tag{27}$$

where "vec()" denotes a reshaping operator that converts a matrix to a column vector, resulting in 210 nonlinear differential equations [8].

The nonlinear constrained optimization was implemented in MATLAB with the use of the function fmincon. The optimization state was comprised of the seven dimensional vector of costates, and the objective function aimed to minimize the absolute value of the difference between the initial spacecraft wet mass and the mass at the end of the transfer: $|m_0 - m(t_f)|$, thus minimizing spent fuel mass. This required integrating the complete trajectory and all 210 nonlinear ODEs each time the function was called. Likewise, the nonlinear constraint function passed into fmincon did this as well, where instead this function was an implementation of the shooting function, $\Psi(\boldsymbol{\lambda})$. The integrator used was a fixed-step Runge-Kutta fourth order scheme with relative and absolute tolerances both set to 1×10^{-10}. All of the numerical computations were performed on a Macbook Pro with M1 Pro processor with macOS Monterey and 32 GB of RAM.

IV. Results & Discussion

In the original formulation of the problem, a target point was chosen on the halo at random. Through trial and error, a time of flight of 140 days was selected. As a first step, the energy optimal trajectory was the focus. The optimization took roughly 6 hours to run until fmincon eventually timed out due to lack of convergence at the step tolerance. Randomized initial seed values for the costates were provided in successive runs with similar performance. This lack of convergence is not to be unexpected, though. The optimizer is tasked with searching through the hypersphere of $\mathbb{R}^7$, which is an unfathomably large search space. In an attempt to constrain the upper and lower bounds of the costates, a large sample

Table 2 Boundary Conditions

Boundary condition	Value
Initial position, $\mathbf{r}_0$	[0.999928426013214, -0.000273918724871, 0.000000004748913]^T DU
Initial velocity, $\mathbf{v}_0$	[0.099829171242128, -0.024990393722611, 0.000004690810464]^T VU
Final position (halo), $\mathbf{r}_f$	[1.008953576065918, 0.005202255493608, -0.000412795563371]^T DU
Final velocity (halo), $\mathbf{v}_f$	[0.003423789025103, 0.000391316565629, -0.005172129644120] ^{T} VU
Final position (manifold), $\mathbf{r}_f$	[1.000747442730326, -0.000540471999299, -0.000644000384683]^T DU
Final velocity (manifold), $\mathbf{v}_f$	[0.058351174289257, -0.017418777627380, -0.030014283539712]^T VU

of N=10,000 7-dimensional uniformly-distributed random costate vectors were generated on the interval of [-1,1], except for the mass costate which was strictly positive due to the problem definition, and fed to the nonlinear constraint function. If the feasibility, approximated as the infinity-norm of the equality constraints vector, returned a value less than 1e-5, then the associated costates were fed back into the optimizer as a new seed. The results of this method can be seen in Fig.8. This is the closest trajectory that was able to acquired for a direct halo-insertion. It is obvious that this transfer completely misses the target point, meanwhile following what appears to be an energetic escape trajectory.

After spending a lot of time tweaking parameters and configurations, the method of target acquisition was switched such that the terminal state changed from the halo now to the stable manifold leading to the original point on the halo. The stable manifold was propagated in backwards in time until it was within 4 GEO orbital radii from the Earth, or about 0.001 DU. This time was approximately 120 days. The time of flight for the controlled leg of the transfer was adjusted to 40 days as to not overshoot this closer target. Unfortunately, the optimizer still failed to converge onto a feasible energy-optimal solution. The closest trajectory which employed manifold-shooting can be seen in Fig.9.

As mentioned earlier, the largest hindrance in this optimization problem is the unconstrained nature of the search space, making the selection of seemingly random points in $\mathbb{R}^7$ a Sisyphean task with the current naive implementation. Many other sources have recognized the issues with this selection method and have thus implemented other solutions which impose constraint the search space and/or constraints on the trajectory itself [1, 8, 10, 13, 14]. A robust approach employed by Chikine (2019) called multiple shooting discretizes the trajectory into an integer number of k stages, then imposes additional boundary conditions such that the terminal conditions of the i^{th} stage are the initial conditions for its neighboring stage, $i + 1$, thus reformulating the problem into a multi-point boundary value problem (MPBVP) up from the simpler TPBVP [13]. Jiang, Baoyin, et al. (2012) used a particle swarm optimization (PSO) technique which is an evolutionary search algorithm that is designed to aid in the global search of unknown parameters for nonlinear optimization, even in the absence of gradient information [10].

In the future, it would be interesting to explore these more robust implementations as well as parallelizing the search algorithm via use of a local server to reduce computational load.

V. Conclusions

In this report, a formulation of the low-thrust-controlled circular restricted three body problem is presented with the goal of designing fuel-optimal transfers to enable the refueling of spacecraft in orbit about Sun-Earth L_2. The optimal control problem is presented as a two-point boundary value problem which is then reformulated into the corresponding initial value problem with indirect shooting procedure to determine the initial costates. The fuel-optimal control structure takes the form of bang-bang control, leading to discontinuities in the numerical integration of the equations of motion. To remedy this, two forms of smoothing were implemented, namely fuel-energy homotopy and hyperbolic tangent smoothing, to allow for a continuous transition between the energy-optimal solution and the fuel-optimal solution while also ensuring continuous differentiability everywhere on the domain of the throttle control input. Terminal conditions for the optimization were first selected as an arbitrary point on the nominal halo orbit for the James Webb Space Telescope. After many trials of failed convergence with this point, the associated stable manifold was propagated backwards in time towards the initial GEO orbit of the refueling spacecraft where the terminal conditions are then relocated. Naive implementation of a randomized costate search procedure maintained the failed convergence status despite changing targets.

Acknowledgments

I would like to thank Prof. Dmitry Savransky for his guidance over the course of this project. I would also like to thank Grace Genszler for discussing difficulties of the project with me as well as offering up helpful suggestions on how to move forward.

References

[1] Woollands, R., and Eggl, S., "Optimal Low Thrust Orbit Transfers for Space Telescope Refueling at SEL2," 2020.

[2] Savransky, D., "The Three Body Problem," , 2022. Course materials for MAE 6720/ASTRO 6579 at Cornell University.

[3] Koon, W., Lo, M., Marsden, J., and Ross, S., *Dynamical Systems, the Three-Body Problem and Space Mission Design*, 2011.

[4] Kolemen, E., Kasdin, N. J., and Gurfil, P., "Multiple Poincaré sections method for finding the quasiperiodic orbits of the restricted three body problem," *Celestial Mechanics and Dynamical Astronomy*, Vol. 112, No. 1, 2012, pp. 47–74.

[5] Gomez, G., Jorba, A., Masdemont, J. J., and Simo, C., *Dynamics And Mission Design Near Libration Points, Vol III: Advanced Methods For Collinear Points*, Vol. 4, World Scientific, 2001.

[6] Richardson, D. L., "Analytic construction of periodic orbits about the collinear points," *Celestial mechanics*, Vol. 22, No. 3, 1980, pp. 241–253.

[7] Howell, K. A. C., *Three-dimensional, periodic halo orbits in the restricted three-body problem*, Stanford University, 1983.

[8] Zhang, C., Topputo, F., Bernelli-Zazzera, F., and Zhao, Y.-S., "Low-thrust minimum-fuel optimization in the circular restricted three-body problem," *Journal of Guidance, Control, and Dynamics*, Vol. 38, No. 8, 2015, pp. 1501–1510.

[9] Bertrand, R., and Epenoy, R., "New smoothing techniques for solving bang–bang optimal control problems—numerical results and statistical interpretation," *Optimal Control Applications and Methods*, Vol. 23, No. 4, 2002, pp. 171–197.

[10] Jiang, F., Baoyin, H., and Li, J., "Practical techniques for low-thrust trajectory optimization with homotopic approach," *Journal of guidance, control, and dynamics*, Vol. 35, No. 1, 2012, pp. 245–258.

[11] Savransky, D., "Numerical Methods," , 2022. Course materials for MAE 6720/ASTRO 6579 at Cornell University.

[12] Geipel, E., "HALO Orbit Determination, Integration, and Station Keeping," Ph.D. thesis, Purdue University, 2019.

[13] Chikine, S., "Low-Thrust Trajectory Optimization in the Circular Restricted Three Body Problem," Ph.D. thesis, University of Colorado at Boulder, 2019.

[14] Yasin, A., "Trajectory Optimization to send a mission in Halo Orbit about L2 Libration Point in Earth-Moon System," Ph.D. thesis, Institute of Space Technology, 2015.

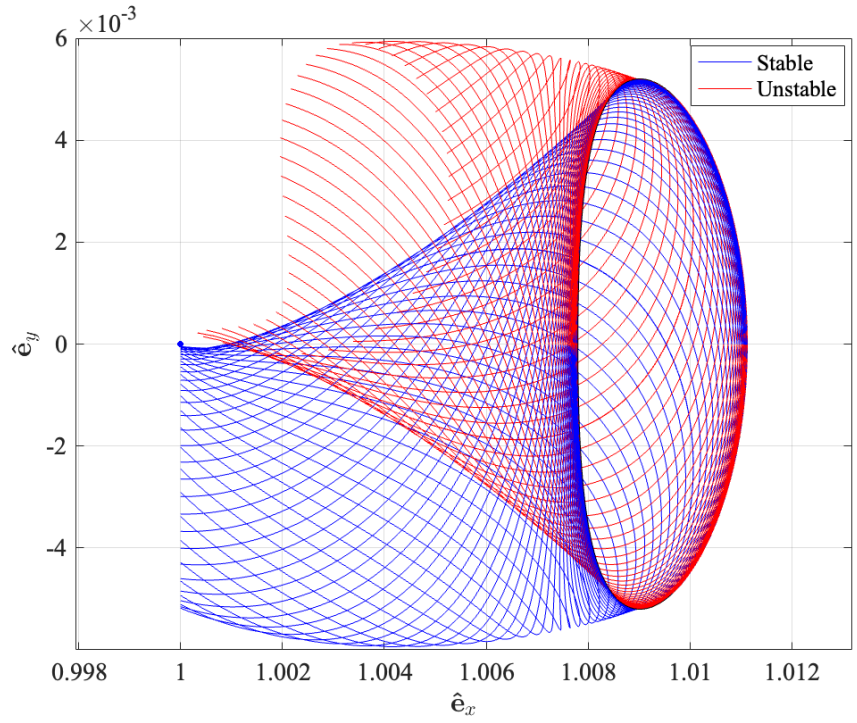

(a)

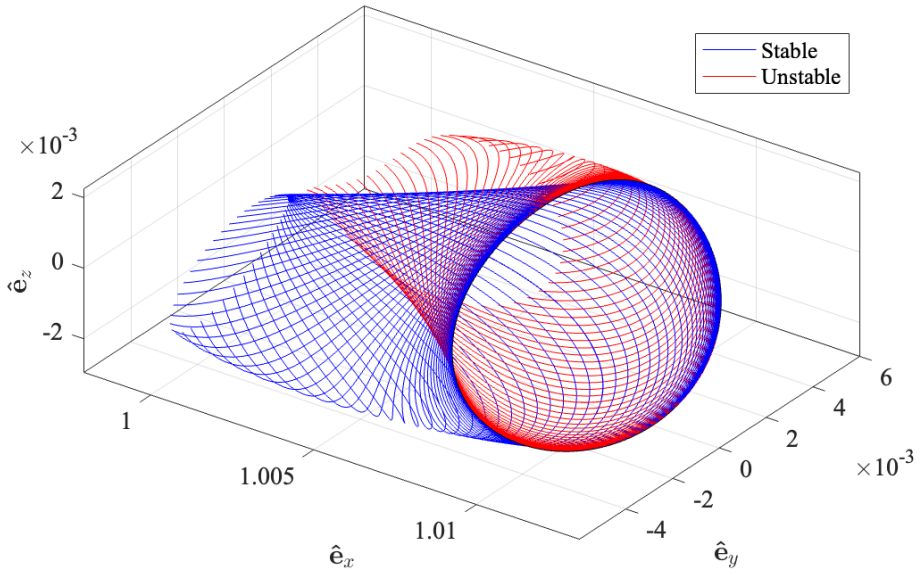

(b)

Fig. 7 (a) Top and (b) side views of generated stable (blue) and unstable (red) manifolds.

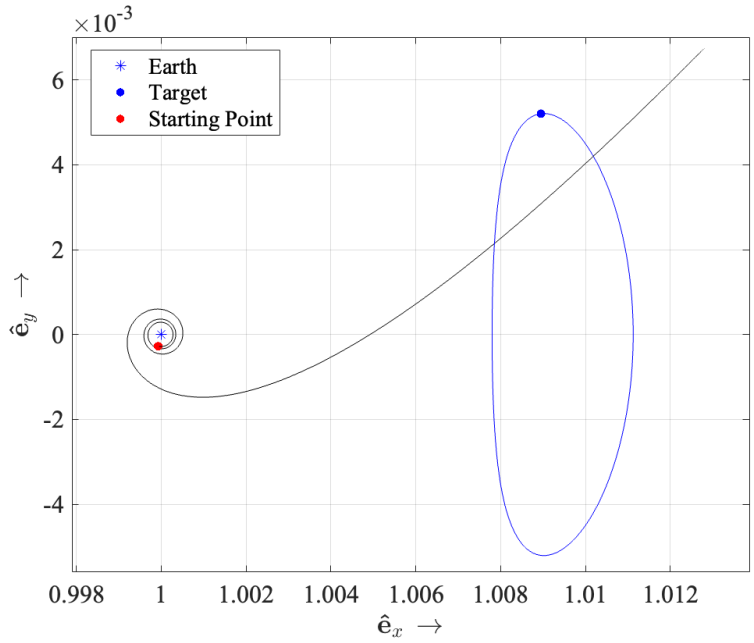

Fig. 8 Most optimal halo-shooting transfer acquired shows failed convergence on the terminal boundary conditions.

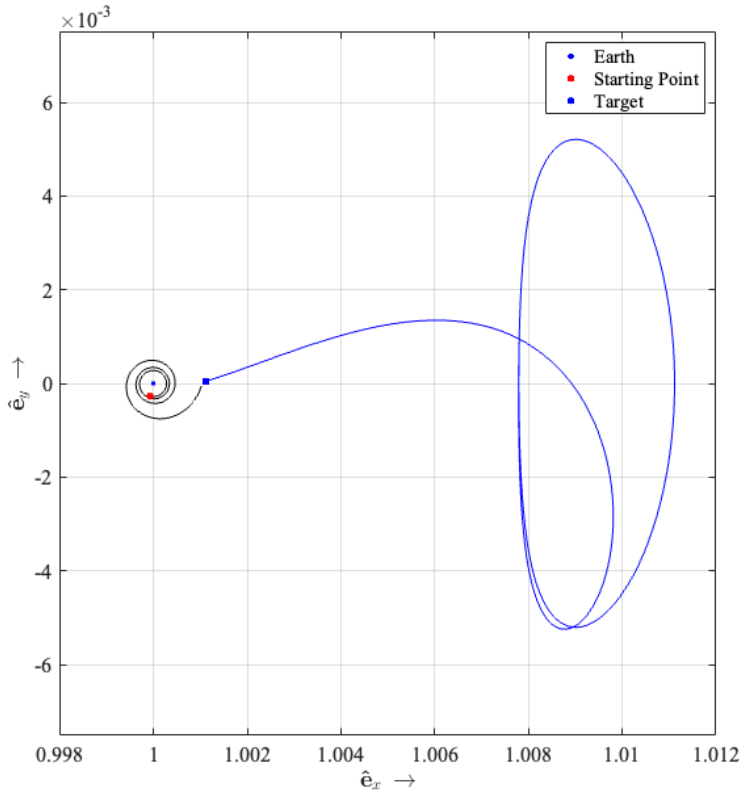

Fig. 9 Most optimal manifold-shooting transfer acquired shows small delta in position with target point, but there is still a noticeable discrepancy in velocity per the angle of arrival at the target.